

**The Detection of Massive Molecular Complexes
in the Ring Galaxy System Arp 143**

James L. Higdon¹

CSIRO/Australia Telescope National Facility

Paul Wild Observatory

Locked Bag 194, Narrabri, NSW 2390

E-mail: jhigdon@atnf.csiro.au

Richard J. Rand

Department of Physics and Astronomy

University of New Mexico

800 Yale Blvd, NE

Albuquerque, NM 87131

E-mail: rjr@gromit.phys.unm.edu

and

Steven D. Lord

IPAC/Caltech, MS 100-22

Pasadena, CA 91125

E-mail: lord@ipac.caltech.edu

¹ATNF Fellow

Received _____; accepted _____

ABSTRACT

We have imaged the kpc scale distribution of $^{12}\text{CO}(J=1-0)$ emission in the ring galaxy system Arp 143 (NGC 2444/2445) using the OVRO millimeter array. We find two giant molecular complexes in the ring component (NGC 2445) and a bright central source. The ring complexes represent 20–60% of the detected M_{H_2} , depending on the relative $I_{CO}-N_{H_2}$ for the ring and nucleus. Their individual H_2 masses and surface densities (Σ_{H_2}) exceed typical spiral arm GMAs regardless of the conversion factor. Both are associated with a 6 kpc ridge of peak Σ_{HI} and massive star formation (MSF) activity. $H\alpha$ imaging shows a patchy ring of HII regions situated along the outer edge of the HI ring. The kinematics of the HI ring show clear signs of expansion. A simple rotating-expanding ring model ($V_{exp} = 118 \pm 30 \text{ km s}^{-1}$) fits the data reasonably well, implying a ring age of $\gtrsim 60 \pm 15$ Myrs. NGC 2445’s ring is able to promptly form very large molecular complexes in a metal poor ISM and trigger MSF.

Nearly eighty per cent of the detected $^{12}\text{CO}(1-0)$ flux originates in a resolved central source that is slightly offset from NGC 2445’s starburst nucleus. We find an ordered velocity field in this component. Assuming an inclined disk, we argue that it is dynamically stable. The central Σ_{H_2} ($910 M_{\odot} \text{ pc}^{-2}$) significantly exceeds Σ_{H_2} commonly found in normal spirals, but is much smaller than values derived in similar sized regions of IR luminous galaxies. The nuclear H_2 may be the result of a previous encounter with NGC 2444. $^{12}\text{CO}(1-0)$ emission in ring galaxies may be dominated by the nucleus, which could bias the interpretation of single-dish measurements.

Subject headings: galaxies: individual (Arp 143) – individual (NGC 2445) –

galaxies: interactions – galaxies: ISM – galaxies: starburst – ISM: molecules
– ISM: HI

1. Introduction

HI studies of such archetype ring galaxies as the Cartwheel and AM0644-741 show that $\sim 90\%$ of the neutral atomic ISM is concentrated in the narrow orbit crowded rings for at least 40 Myrs (Higdon 1996; Higdon, Wallin, Staveley-Smith, & Lord 1997). This is thought to create an environment conducive to the formation of massive cloud complexes and the triggering of massive star formation (MSF) through elevated collision rates. However, we know little of the molecular ISM in these systems, which is unfortunate since massive stars in normal galaxies form exclusively in giant molecular clouds and associations (GMAs). Investigations of the molecular component of ring galaxies through the prominent 115 GHz $^{12}\text{CO}(J=1-0)$ transition has proven difficult due to their $\sim 1'$ angular size, which is comparable to the beams of most single-dish mm-wave telescopes, and typically low $^{12}\text{CO}(1-0)$ fluxes (Horellou et al. 1995; Higdon, Lord, & Rand 1997). This has led to speculation that MSF in ring galaxies occurs in a primarily *atomic* ISM (Higdon 1996). In this Letter we present the first aperture synthesis $^{12}\text{CO}(J=1-0)$ observations of a putative ring galaxy system – Arp 143 (NGC 2444/2445), which possesses the largest 115 GHz line flux in our ring galaxy survey. Complementary HI and $\text{H}\alpha$ data are also presented to explore the relationship between the neutral ISM and MSF on similar spatial scales. We will show that NGC 2445 is indeed a young ring galaxy, whose ring is forming unusually large GMAs in a metal poor ISM and triggering MSF.

Optical images of NGC 2445, the Southern component in Arp 143, show a compact nucleus surrounded by a number of blue knots which are in fact low metallicity² HII regions (Burbidge & Burbidge 1959; Jeske 1986). Appleton, Schombert, & Robson (1992) found that most of the knots have optical/NIR colors consistent with very young (Age $\lesssim 10$ Myrs)

² $12 + \log[\text{O}/\text{H}] = 8.56-8.77$, Jeske (1986).

stellar populations, and are located along the outer edge of an HI crescent, the distribution expected in ring galaxies created in an off-centered “intruder” passage. They proposed that NGC 2445 represented a young “pre-starburst” ring galaxy. The HI crescent’s kinematics were not discussed, and no ring expansion - the *sine qua non* for a collisional ring galaxy - was reported. We presented $^{12}\text{CO}(1-0)$ single-dish results for Arp 143 in Higdon et al. (1995) and noted an enhancement in line emission Northwest of NGC 2445’s nucleus. We proposed that this was due to molecular gas in the HI crescent.

2. Observations and Data Reduction

$^{12}\text{CO}(J=1-0)$ observations of Arp 143 were made using the six-element Owens Valley Radio Observatory millimeter-wave interferometer on 2 & 20 May 1995 in the compact “A” configuration (20.8–200 m baseline range). Each 10.4 m antenna was equipped with an SIS receiver cooled to 4 K. Single sideband T_{sys} were between 300–500 K at 113 GHz. The correlator was configured for 120 channels separated by 2 MHz (5.2 km s^{-1}), giving a usable velocity range of 660 km s^{-1} . The array tracked a position near NGC 2445’s optical nucleus for two 12-hour runs. Time dependent amplitude and phase variations were monitored through frequent observations of QSO 0642+449, while 3C 273 was used to define the flux scale and correlator bandpass shape. We estimate the flux calibration uncertainty to be 10%. The UV data were processed using the OVRO reduction package MMA (Scoville et al. 1992). Channel maps were made using both natural ($\theta_{FWHM} = 5''$, $1\sigma = 12 \text{ mJy beam}^{-1}$, $\Delta V = 10.4 \text{ km}^{-1}$) and uniform ($\theta_{FWHM} = 3.9''$, $1\sigma = 14 \text{ mJy beam}^{-1}$, $\Delta V = 20.8 \text{ km}^{-1}$) weighting in AIPS, and CLEANed. The naturally weighted maps were further convolved to increase sensitivity ($\theta_{FWHM} = 8''$, $1\sigma = 10 \text{ mJy beam}^{-1}$). At the assumed distance of 40 Mpc ($H_o = 100 \text{ km s}^{-1} \text{ Mpc}^{-1}$) this corresponds to a spatial resolution of 1.6 kpc. Integrated $^{12}\text{CO}(1-0)$ maps were made by summing emission that exceeded the 3σ

map noise, showed spatial and velocity continuity over at least 3 consecutive channels, and was within 150 km s^{-1} of the local HI velocities. The final maps were corrected for primary beam attenuation. No continuum emission was detected.

Arp 143 was observed with the Very Large Array³ on 27 December 1995 in B-configuration to image HI emission with velocity and spatial resolution comparable with the OVRO data. Details of those observations will be presented elsewhere. Naturally weighted channel maps ($\theta_{FWHM} = 5.4''$, $1\sigma = 0.3 \text{ mJy beam}^{-1}$, $\Delta V = 10.6 \text{ km s}^{-1}$) were used to construct HI moment maps using routines in AIPS. IDL programs were used to analyze the HI kinematics.

We obtained $H\alpha + [\text{N II}]$ and Johnson B-band CCD images of Arp 143 with the McDonald Observatory 0.76 m telescope on 10-12 March 1992 using the TI2 CCD located at the Cassegrain focus ($0.58'' \text{ pix}^{-1}$). Line emission was isolated using an 80 \AA FWHM filter centered at 6650 \AA , while line-free continuum was mapped using a wider (120 \AA FWHM) filter centered blueward of $H\alpha$. The CCD reduction was routine and performed in IRAF. The line map was calibrated using extinction corrected HII region line fluxes from Jeske (1986), and is believed accurate to $\sim 25\%$, except in the nucleus where the images saturate. The $H\alpha$ image was smoothed ($\theta_{FWHM} = 5''$) to improve sensitivity and better match the $^{12}\text{CO}(1-0)$ and HI data. Measured field star positions were used to define an astronomical coordinate system in the optical images to an accuracy of $1''$ (Benedict & Shelus 1978).

3. Results

³The National Radio Astronomy Observatory is a facility of the National Science Foundation operated under cooperative agreement by Associated Universities, Inc.

3.1. The Neutral ISM of NGC 2445

Contours of integrated $^{12}\text{CO}(1-0)$ and HI line intensity are shown superposed on the Arp 143 B-band image in Figures 1a & b. We find $(1.25 \pm 0.08) \times 10^9 M_{\odot}$ of atomic hydrogen concentrated into an ~ 15 kpc diameter ring in NGC 2445’s disk. Though we detect only 25% of the single-dish 21cm flux (Shostak 1978), our data provides a high resolution view of the HI ring, the most conspicuous component in Appleton et al.’s (1992) C- and D- array VLA maps. The highest Σ_{HI} is found in a quasi-linear ridge West of the ring’s optical nucleus ($30\text{--}60 M_{\odot} \text{ pc}^{-2}$). Surface densities between 3 and $20 M_{\odot} \text{ pc}^{-2}$ typify the rest of the HI crescent. We do not detect HI in NGC 2445’s nucleus or in NGC 2444. By contrast, $^{12}\text{CO}(1-0)$ emission in NGC 2445 is dominated by a slightly resolved nuclear source, plus two large complexes (“a” & “b”) $\sim 20''$ to the West & Northwest. Both are associated with the ring’s high Σ_{HI} ridge. A third elongated source (“c”) extends Southeast from the nucleus into a low Σ_{HI} region. Their emission properties are listed in Table 1. Altogether, we measure a $^{12}\text{CO}(1-0)$ flux integral of $36.7 \pm 2.1 \text{ Jy km s}^{-1}$ within the OVRO primary beam, or 33% of the single-dish value (Higdon et al. 1995). Adopting a Galactic $I_{CO}\text{--}N_{H_2}$ conversion factor (X_{Gal} , Bloemen et al. 1986) leads to a total H_2 mass of $(1.2 \pm 0.1) \times 10^9 M_{\odot}$. But given the LMC-like metallicity of the ring, use of an LMC conversion factor (X_{LMC} , Cohen et al. 1988) may be more appropriate for “a” and “b”, in which case the total M_{H_2} becomes $(2.2 \pm 0.2) \times 10^9 M_{\odot}$. The two ring GMAs would then represent 60% of the total molecular gas detected by the array. We will dodge the uncertain conversion factor issue by listing a range of M_{H_2} and Σ_{H_2} corresponding to the two choices of X.

The two molecular complexes of the ring contribute 19% of the observed $^{12}\text{CO}(1-0)$ emission. Their individual H_2 masses are $1.6\text{--}9.7 \times 10^8 M_{\odot}$ (“a”) and $0.4\text{--}2.5 \times 10^8 M_{\odot}$ (“b”). Compared with the GMAs in M100 and M51, mapped with 700 pc resolution by

Rand (1995, 1993), NGC 2445’s complexes are more massive with a comparable range in Σ_{H_2} assuming X_{Gal} (Table 1). NGC 2445’s Σ_{H_2} ’s are no doubt lower limits due to the 1.6 kpc naturally weighted synthesized beam. At higher resolution they might break up into less massive GMAs as well. However, if X_{LMC} applies, their M_{H_2} and Σ_{H_2} significantly exceed the GMAs in M100 & M51, even when making allowances for differing resolutions. Both “a” and “b” are found in high Σ_{HI} regions ($\sim 50\text{-}60 M_{\odot} \text{pc}^{-2}$), though HI and $^{12}\text{CO}(1\text{-}0)$ peaks do not coincide. Regions where $\Sigma_{HI} > 20 M_{\odot} \text{pc}^{-2}$ and where no $^{12}\text{CO}(1\text{-}0)$ emission is detected are found within the OVRO primary beam. H_2 may of course be present here as our map noise sets a point source M_{H_2} detection limit of $1.8 \times 10^7 M_{\odot}$ (3σ) for ΔV of 30 km s^{-1} and X_{Gal} . Significant differences between the $^{12}\text{CO}(1\text{-}0)$ and HI velocities were found in the ring, with ΔV_{CO-HI} equal to -38 km s^{-1} for “a” and $+40 \text{ km s}^{-1}$ for “b”. Both are located in regions of large HI velocity dispersion or streaming, so it is difficult to attribute the offsets to an obvious systematic effect.

More than 80% of the total $^{12}\text{CO}(1\text{-}0)$ flux, or $(7.1 \pm 1.6) \times 10^8 M_{\odot}$ of H_2 (X_{Gal}), is emitted by NGC 2445’s nucleus. The $^{12}\text{CO}(1\text{-}0)$ peak is displaced $5''$ (0.8 kpc) Southwest of the optical center. A uniformly weighted $^{12}\text{CO}(1\text{-}0)$ map of this region is presented in Figure 2a, and shows the emission to be clearly elongated along a position angle of 71° , with a minor/major axis ratio of $\sim 2/3$. NGC 2445’s peak Σ_{H_2} ($910 M_{\odot} \text{pc}^{-2}$, X_{Gal}) is significantly larger than Σ_{H_2} inferred in the nuclei of normal spirals ($\overline{\Sigma}_{H_2} = 190 M_{\odot} \text{pc}^{-2}$ in 8 Virgo spirals, with an $88 M_{\odot} \text{pc}^{-2}$ rms, Canzian 1990) and some mergers (e.g., NGC 4038/39, Stanford et al. 1990). However, NGC 2445’s central M_{H_2} and Σ_{H_2} are far outclassed by the centers of IR luminous galaxies like Mrk 273 ($\Sigma_{H_2} = 3.8 \times 10^4 M_{\odot} \text{pc}^{-2}$, Yun & Scoville 1995). These comparisons are summarized in Table 1.

The velocity field of the nuclear $^{12}\text{CO}(1\text{-}0)$ emission (Figure 2b) shows ordered motions suggesting a disk geometry. We estimated its dynamical mass assuming a radius of 490 pc

and $45^\circ \pm 10^\circ$ inclination to be

$$M_{dyn} = \frac{R V_{1/2}^2}{G \sin^2 i} = (3.3 \pm 1.3) \times 10^9 M_\odot. \quad (1)$$

The ratio of molecular to dynamical mass M_{H_2}/M_{dyn} is 0.2 ± 0.1 using X_{Gal} , and is consistent with a system in equilibrium given the uncertainties. This is also similar to values determined for the nuclei of normal spirals, as opposed to the molecular masses and M_{H_2}/M_{dyn} typically found in IR luminous galaxies (Yun et al. 1994). Finally, we tentatively identify the elongated source “c” with a faint dust lane visible in the Arp Atlas (1966) photograph.

3.2. Massive Star Formation and the ISM in NGC 2445

Figure 1c shows the distribution of HII regions in Arp 143 with $L_{H\alpha}$ between 0.6 - 15. $\times 10^{39}$ erg s^{-1} . All are found in NGC 2445. Apart from the nucleus, MSF is concentrated along a patchy ellipse having the same general shape as the HI crescent in Figure 1b. The 3 most luminous HII regions form an ~ 6 kpc complex associated with both the GMAs “a” & “b” and the high Σ_{HI} ridge of the ring. We estimate the ring’s SFR to be $0.5 M_\odot \text{ yr}^{-1}$ based on its $L_{H\alpha}$, which is 25% of the nuclear SFR (Kennicutt 1983, Jeske 1986). This is only 25% of the average SFR for four similarly sized ring galaxies in Marston & Appleton’s (1995) survey, and less than 1% of the Cartwheel’s (Higdon 1995). The global relationship between HI, $^{12}\text{CO}(1-0)$, and $H\alpha$ emission is illustrated in Figure 1d. Note that with one exception HII regions are situated along the outer edge of the $\Sigma_{HI} > 10 M_\odot \text{ pc}^{-2}$ ring. This is most pronounced in the South and East, but is also true in the HI ridge West of the nucleus. We detect no HII regions with $L_{H\alpha}$ above 3×10^{38} erg s^{-1} (3σ) in NGC 2445 apart from the nucleus and ring, or in NGC 2444.

3.3. Kinematics of the HI Ring

In Figure 3 we show a radial velocity-position angle diagram for the HI ring. The data represent averages within 10° segments of a $6''$ wide annulus fit to the HI distribution. The dashed line shows the best fit to a *non-expanding* rotating circular ring model. Strong non-circular motions are seen along the minor axis on both sides of the ring (p.a. = $40\text{-}130^\circ$ and $250\text{-}340^\circ$) which are most easily explained as expansion. The solid line shows a least-squares fit of a rotating-expanding circular ring model, from which we derive $V_{sys} = 4000 \pm 10 \text{ km s}^{-1}$, $V_{rot} = 214 \pm 25 \text{ km s}^{-1}$, and $V_{exp} = 118 \pm 30 \text{ km s}^{-1}$. The rotating-expanding ring is not a perfect fit. This may reflect non-planar motions, tidal interaction with NGC 2444, or departures from circularity. Note that the largest discrepancy occurs near p.a. = 180° , which is where the HI ring splits in two. Nevertheless, expansion is clearly indicated by the data. From the ring’s radius and V_{exp} we estimate its age to be $\sim 60 \pm 15 \text{ Myrs}$, or 20% of the Cartwheel’s (Higdon 1996).

4. Discussion

These observations show that NGC 2445’s ring contains large scale concentrations of molecular gas. At 1.6 kpc resolution, their M_{H_2} and Σ_{H_2} appear larger than those typically found in spiral arms, especially if X_{LMC} is adopted. Their close association with the highest Σ_{HI} of the ring suggests their formation in the orbit crowded ring density wave through agglomeration or gravitational instability. The ring is clearly capable of forming large molecular masses out of a metal poor ISM. Similarly, the concentration of luminous metal poor HII regions along the gas ring’s outer edge, and the close association between peak Σ_{HI} , Σ_{H_2} , and $\Sigma_{H\alpha}$ implies direct MSF triggering, rather than the simple rearrangement of pre-existing star forming regions (Higdon 1995).

We find the morphology of NGC 2445’s neutral and ionized gas to be in excellent agreement with model ring galaxies formed in off-centered collisions (cf. Appleton & Struck 1987). Indeed, the absence of a stellar bar makes it very unlikely that the gas ring is a resonance phenomenon. We found strong evidence of expansion in the HI ring implying that the ring was formed $\gtrsim 60 \pm 15$ Myrs ago. Together with the ring’s low metallicity and ~ 10 Myr old clusters, the large M_{H_2} and Σ_{H_2} for complexes “a” and “b”, and a low SFR relative to other rings, the body of evidence points to NGC 2445 being a young ring galaxy.

The origin of the nuclear $^{12}\text{CO}(1-0)$ emission is less certain. The high Σ_{H_2} relative to normal spirals coupled with the nuclear starburst suggest a tidal origin. However the central Σ_{H_2} is clearly not in the same class as IR luminous galaxies. Published ring galaxy simulations do produce large mass buildups in central regions, but not until the ring galaxy is highly evolved (e.g., Appleton & Struck 1987, Mihos & Hernquist 1994). Appleton et al. (1987) found a narrow HI plume extending $\gtrsim 100$ kpc from Arp 143. Such a large structure should be much older than the ~ 60 Myr old ring, implying multiple interactions between NGC 2444 and 2445. It is conceivable that a large impact parameter encounter generated the long HI tidal tail, while at the same time funneling gas to the center of NGC 2445. This lowered the total orbital energy sufficiently to bring NGC 2444 through the disk of NGC 2445 ~ 60 Myrs ago, forming the ring. Recent models suggest that the nuclear gas would be able to survive NGC 2444’s “intrusion”, especially if the latter were gas poor (Struck 1997). The next encounter will likely lead to a merger of the two galaxies. These issues should be explored further with detailed numerical simulations.

Regardless of its origin, there is evidence that nuclear components may dominate the molecular emission of ring galaxies. Of the 6 ring galaxies large enough to be observed with multiple pointings by Horellou et al. (1995), $^{12}\text{CO}(1-0)$ emission peaked at the nucleus in each case. If this is true in general, comparisons between global H_2 properties derived

using low resolution single-dish measurements and optical H α or B-band fluxes may not be very meaningful, since young stars are highly concentrated in the outer rings. Unless emission from the nucleus and rings can be distinguished, the analysis may be subject to large systematic errors. $^{12}\text{CO}(1-0)$ interferometric studies of other ring galaxies are clearly needed. However, the best examples of this class such as the Cartwheel will require the next generation of millimeter-wave arrays.

We wish to thank Curt Struck for a number of enlightening discussions, Philip Appleton for the use of his H α filter, and B. Canzian for access to some of his unpublished results on Virgo Cluster spirals. A special word of thanks is also extended to the staffs at the Owens Valley Radio Observatory, McDonald Observatory, and NRAO for their help and support. We also wish to thank an anonymous referee for suggesting a number of improvements. This research has made use of the NASA/IPAC Extragalactic Database (NED) which is operated by the Jet Propulsion Laboratory, California Institute of Technology, under contract with the National Aeronautics and Space Administration.

REFERENCES

- Appleton, P. N., & Struck, C. 1987, *ApJ*, 318, 103
- Appleton, P. N., Schombert, J. M., & Robson, E. I. 1992, *ApJ*, 385, 491
- Appleton, P. N., Ghigo, F. G., Van Gorkom, J. H., Schombert, J. M., & Struck, C. 1987, *Nature*, 330, 140
- Arp, H. J. 1966, *ApJS*, 14, 1
- Benedict, G. F., & Shelus, P. J. 1978, Applications of Automated Inventory Techniques to Astrometry, in *Proceed. I. A. U. Colloquium No. 48*, 109
- Bloemen, J. B., Strong, A. W., Blitz, L., Cohen, R. S., Dame, T. M., Grabelsky, D. A., Hermsen, W., Lebrun, F., Mayer-Hasselwander, H. A., & Thaddeus, P. 1986, *A&A*, 154, 25
- Burbidge, E. M., & Burbidge, G. R. 1959, *ApJ*, 10, 12
- Canzian, B. 1990, Ph. D. Thesis, California Institute of Technology
- Cohen, R. S., Dame, T. M., Garay, G., Montani, J., Rubio, M., & Thaddeus, P. 1988, *ApJ*, 331, L95
- Higdon, J. L. 1995, *ApJ*, 455, 524
- Higdon, J. L. 1996, *ApJ*, 467, 241
- Higdon, J. L., Smith, B. J., Lord, S. D., & Rand, R. J. 1995, *ApJ*, 438, L79
- Higdon, J. L., Lord, S. D., & Rand, R. J. 1997, in preparation
- Higdon, J. L., Wallin, J. F., Staveley-Smith, L., & Lord, S. D. 1997, in preparation
- Horellou, C., Casoli, F., Combes, F., & Dupraz, C. 1995, *A&A*, 298, 743
- Jeske, N. A. 1986, Ph. D. Thesis, University of California, Berkeley
- Kennicutt, R. A. 1983, *ApJ*, 272, 54

- Marston, A., & Appleton, P. N. 1995, *AJ*, 109, 1002
- Mihos, J. C., & Hernquist, L. 1994, *ApJ*, 473, 611
- Rand, R. J. 1993, *ApJ*, 404, 593
- Rand, R. J. 1995, *AJ*, 109, 2444
- Sanders, D. B., & Mirabel, I. F. 1996, *ARA&A*, 34, 749
- Scoville, N. Z., Carlstrom, J. C., Chandler, C. J., Phillips, J. A., Scott, S. L., Tilanus, R. P., & Wang, Z. 1992, *PASP*, 105, 1482
- Shostak, G. S. 1978, *A&A*, 68, 321
- Stanford, S. A., Sargent, A., Sanders, D. B., & Scoville, N. Z. 1990, *ApJ*, 349, 492
- Struck, C. 1997, private communication
- Yun, M. S., Scoville, N. Z., & Knop, R. A. 1994, *ApJ*, 430, L109
- Yun, M. S., & Scoville, N. Z. 1995, *ApJ*, 451, L45

Figure Captions

Figure 1. – (a) Contours of integrated $^{12}\text{CO}(1-0)$ emission (natural weighting, $\theta_{FWHM} = 8''$) superposed on a B-band CCD image of the Arp 143 system. The dashed circle indicates the OVRO primary beam FWHM. The levels are logarithmic and correspond to 0.45, 0.79, 1.4, 2.5, 4.5, 7.9, 14.1, & 25.1 Jy km s $^{-1}$ beam $^{-1}$. (b) Contours of Σ_{HI} from the VLA B-array data ($\theta_{FWHM} = 5.4''$). The levels range from 10 to 50 M_{\odot} pc $^{-2}$ in steps of 10 M_{\odot} pc $^{-2}$. Crosses mark the positions of HII region centers. (c) Contours of $\Sigma_{H\alpha}$ in Arp 143. Ten logarithmically spaced levels between 7.4 and 340. $\times 10^{-17}$ erg s $^{-1}$ cm $^{-2}$ arcsec $^{-2}$ are shown. (d) Composite showing relative distribution of Σ_{HI} (grey scale), Σ_{CO} (contours), and HII regions (crosses).

Figure 2. – Molecular gas in NGC 2445’s nucleus using the uniformly weighted OVRO data ($\theta_{FWHM} = 3.9''$). (a) Contours of integrated $^{12}\text{CO}(1-0)$ emission from 2.3 to 20.7 Jy km s $^{-1}$ beam $^{-1}$ in steps of 2.3 Jy km s $^{-1}$ beam $^{-1}$. The cross marks the center of the optical nucleus. (b) Flux-weighted velocity field. The contours are labeled in units of km s $^{-1}$ (optical-Heliocentric).

Figure 3. – Radial velocity-position angle diagram for the HI ring shown in Figure 1b. Position angle increases counterclockwise from the Eastern major axis line of nodes. The solid line represents a least-squares fit to an inclined circular, rotating, and expanding ring model, while the dashed line corresponds to the same model without expansion. The rotating-expanding model gives $V_{sys} = 4000 \pm 10$ km s $^{-1}$, $V_{rot} = 214 \pm 25$ km s $^{-1}$, and $V_{exp} = 118 \pm 30$ km s $^{-1}$.

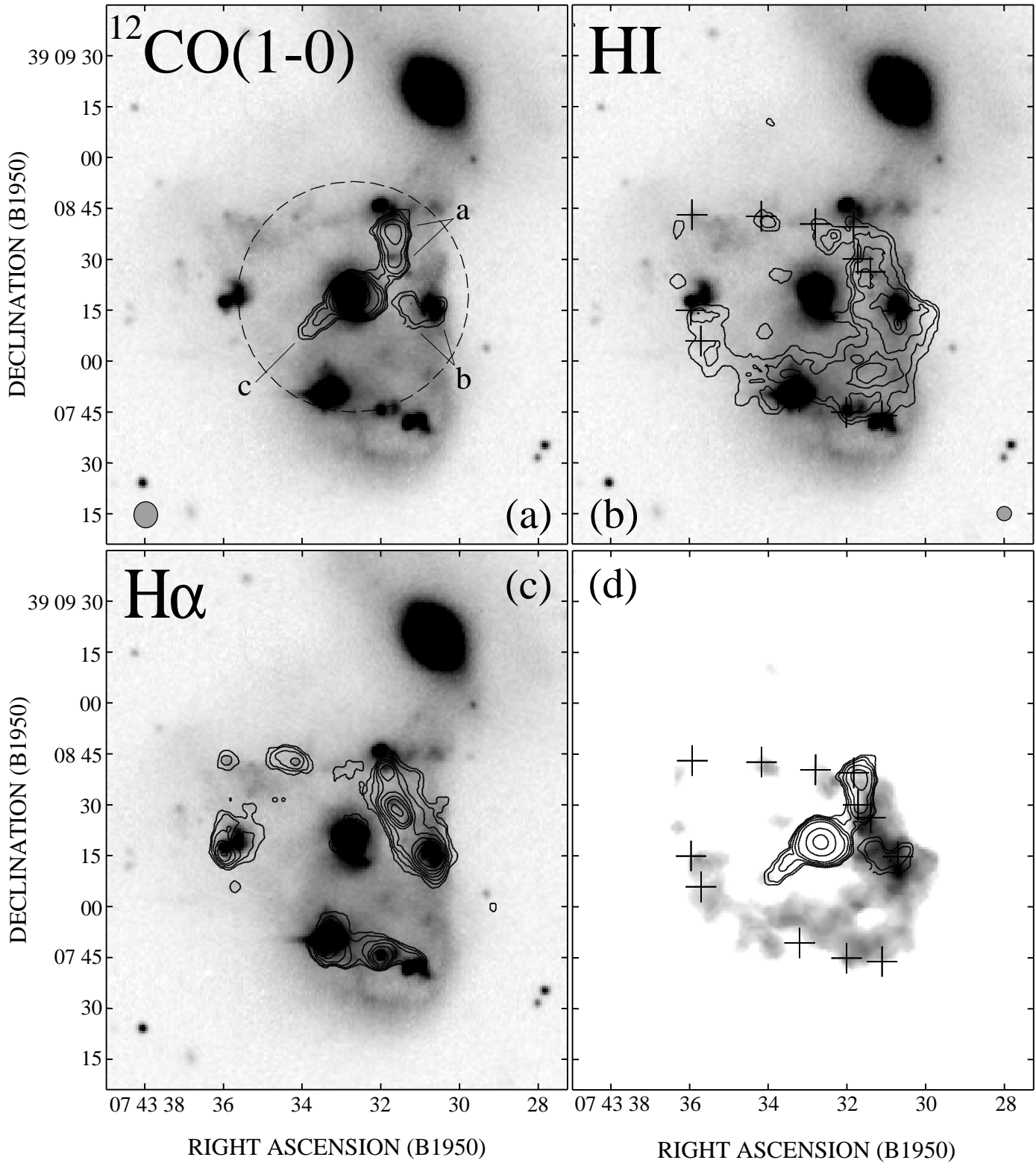


TABLE 1
MOLECULAR GAS PROPERTIES

Region	$\int S dv$ (Jy km s ⁻¹)	M_{H_2} ^a (10 ⁷ M _⊙)	Σ_{H_2} ^a (M _⊙ pc ⁻²)	ΔV_{FWZI} (km s ⁻¹)
Arp 143 “a”	6.2 ± 0.3	16.–97.	>52.–315.	93.
Arp 143 “b”	1.6 ± 0.2	4.1–25.	>12.–73.	32.
Arp 143 “c”	1.3 ± 0.2	2.7–16.	>17.–100.	31.
M 100 GMAs ^b	–	~7.	~50.–80.	~10.
M 51 GMAs ^c	–	~3.	~50.–80.	~10.
Arp 143 Nucleus ^d	27.6 ± 1.6	71.	910.	229.
Virgo Spiral Nuclei ^e	–	15.	194.	–
LIR Galaxy Nuclei ^f	–	2000.	~10 ⁵	–

^aThe range of values correspond to use of X_{Gal} and X_{LMC} . An H_0 of 100 km s⁻¹ Mpc⁻¹ is assumed throughout.

^bRand 1995.

^cRand 1993.

^dQuoted values derived from Uniformly weighted data assuming X_{Gal} .

^eAverage of 8 Virgo galaxies, Canzian (1990). Standard deviations for M_{H_2} and Σ_{H_2} are $7.1 \times 10^7 M_{\odot}$ and $88 M_{\odot} pc^{-2}$.

^fAverage of 24 LIR galaxies from Sanders & Mirabel (1996).

